



Boussinesq-type modelling using an unstructured finite element technique

Ole R. Sørensen*, Hemming A. Schäffer, Lars S. Sørensen

DHI Water & Environment, Agern Allé 5, DK-2970, Hørsholm, Denmark

Received 26 March 2003; received in revised form 25 September 2003; accepted 17 October 2003

Abstract

A model for solving the two-dimensional enhanced Boussinesq equations is presented. The model equations are discretised in space using an unstructured finite element technique. The standard Galerkin method with mixed interpolation is applied. The time discretisation is performed using an explicit three-step Taylor–Galerkin method. The model is extended to the surf and swash zone by inclusion of wave breaking and a moving boundary at the shoreline. Breaking is treated by an existing surface roller model, but a new procedure for the detection of the roller thickness is devised. The model is verified using four test cases and the results are compared with experimental data and results from an existing finite difference Boussinesq model.

© 2003 Elsevier B.V. All rights reserved.

Keywords: Boussinesq equations; Finite element method; Unstructured grid; Wave breaking; Surface roller; Run-up

1. Introduction

Within the area of Boussinesq-type modelling, significant progress has been made in the last 10 years. Firstly, a number of new Boussinesq-type equations with improved dispersion characteristics and non-linear properties have been presented. Secondly, the Boussinesq-type models have been extended to the surf zone by inclusion of wave breaking and moving shoreline boundary conditions. Madsen and Schäffer (1999) and Kirby (1997, 2003) give recent reviews of the subject.

Today, Boussinesq-type models can be applied to study waves and currents in a region extending from quite deep water and all the way to the shoreline. To resolve the strongly non-linear phenomena in the surf zone, a very fine horizontal mesh is required, while a much coarser mesh can be used in the offshore region. Traditionally, Boussinesq equations are solved using structured Cartesian meshes and finite difference methods (FDMs). Even with the computers of today, these models are very time-consuming for solving practical problems that include modelling of surf zone dynamics. With the goal of reducing the computational cost, it is desirable to introduce more flexible meshes. Control of node distribution allows for optimal usage of nodes and adaptation of mesh resolution to the relevant physical scales. Flexible meshes can be accomplished in a number of ways, e.g., multi-block

* Corresponding author. Tel.: +45-4516-9200; fax: +45-4516-9292.

E-mail addresses: ors@dhi.dk (O.R. Sørensen), has@dhi.dk (H.A. Schäffer), lss@dhi.dk (L.S. Sørensen).

curvilinear meshes, overlapping meshes, local mesh refinement and unstructured meshes. Examples of the use of curvilinear mesh for solving the Boussinesq equations are given by Shi et al. (2001) and Li and Zhan (2001). The present work is based on unstructured meshes, which gives the maximum degree of flexibility. The use of unstructured meshes also makes it possible to handle problems characterised by computational domains with complex boundaries. When explicit time integration schemes are used the time step is usually determined by the stability limit. The use of coarse mesh in offshore regions and only fine mesh in shallow water makes it possible to use larger time steps and reduces the computational costs.

Since the early 1980s, the unstructured finite element method (FEM) has been successfully applied for solving the shallow water equations (e.g., Löhner et al., 1984; Peraire et al., 1986; Kashiya et al., 1995). The application of the finite element method to Boussinesq-type equations has so far mainly been limited to the classical Boussinesq equations of Peregrine (1967), e.g., Antunes Do Carmo and Seabra-Santos (1996). However, recently, other types of Boussinesq equations have been considered. Langtangen and Pedersen (1998) solved a set of weakly dispersive Boussinesq equations formulated in the depth-averaged velocity potential and the surface elevation. Li et al. (1999, 2000) solved the equations quoted by Beji and Nadaoka (1996) in two dimensions using quadrilateral elements with linear interpolating functions for the velocity components and the surface elevation. Finally, Walkley and Berzins (1999) solved the one-dimensional extended Boussinesq equations of Nwogu (1993), and, recently, they have extended the work to two horizontal dimensions (Walkley and Berzins, 2002). They used linear triangular finite elements for the space discretisation.

In the present paper, we describe a model that solves the Boussinesq-type equations of Madsen and Sørensen (1992) using a finite element technique for the spatial discretisation. These equations contain terms with third-order spatial derivatives of the surface elevation. Hence, to make it possible to use a lower-order finite element approximation, the governing equations are rewritten in a lower-order form by introducing an auxiliary variable and an auxiliary

algebraic equation. The standard Galerkin finite element method with mixed interpolation is applied. Equal-order interpolation as used by, e.g., Li et al. (1999, 2000) and Walkley and Berzins (2002) can exhibit severe spurious modes. Both triangular elements (quadratic interpolation of fluxes and linear interpolation of surface elevation and auxiliary variable) and quadrilateral elements (biquadratic interpolation of fluxes and bilinear interpolation of surface elevation and auxiliary variable) are used. The time integration is performed with an explicit three-step Taylor–Galerkin method.

One of the main differences of the new model compared to previous work using flexible mesh technique to solve the Boussinesq equations is that the model is extended to the surf and swash zone by including wave breaking and a moving boundary at the shoreline. The simplified effects of breaking are included using the surface roller concept (Schäffer et al., 1993; Madsen et al., 1997a,b; Sørensen et al., 1998). In the previous work, the surface rollers were determined using a heuristic, geometrical approach. In the present work, a more practical procedure is devised for the determination of these surface rollers. This new procedure provides a substantial simplification over the previously used technique, while giving almost the same results. The moving boundary is treated numerically by replacing the solid beach by a permeable beach characterised by an extremely small porosity following the work by Madsen et al. (1997a).

This paper is structured as follows: In Chapter 2, the governing equations are rewritten in a form suitable for the finite element approach, and the new procedure for determining the surface roller is described. The numerical solution techniques for the spatial discretisation and the time integration are presented in Chapter 3. In Chapter 4, the model is verified using four cases. Finally, Chapter 5 draws up the conclusion.

2. Governing equations

2.1. Enhanced Boussinesq equations

The present work is based on the enhanced Boussinesq equations presented by Madsen and

Sørensen (1992). The simplified effects of wave breaking are included using the surface roller concept (Schäffer et al., 1993; Madsen et al., 1997a,b; Sørensen et al., 1998). This results in additional convective terms. The governing equations have the following form

$$\frac{\partial \eta}{\partial t} + \frac{\partial P}{\partial x} + \frac{\partial Q}{\partial y} = 0 \quad (1a)$$

$$\begin{aligned} \frac{\partial P}{\partial t} + \frac{\partial}{\partial x} \left(\frac{P^2}{d} \right) + \frac{\partial}{\partial y} \left(\frac{PQ}{d} \right) + gd \frac{\partial \eta}{\partial x} + \frac{\partial R_{xx}}{\partial x} \\ + \frac{\partial R_{xy}}{\partial y} + \frac{\tau_x}{\rho} - \frac{\partial}{\partial x} (dT_{xx}) - \frac{\partial}{\partial y} (dT_{xy}) + \psi_x = 0 \end{aligned} \quad (1b)$$

$$\begin{aligned} \frac{\partial Q}{\partial t} + \frac{\partial}{\partial x} \left(\frac{PQ}{d} \right) + \frac{\partial}{\partial y} \left(\frac{Q^2}{d} \right) + gd \frac{\partial \eta}{\partial y} + \frac{\partial R_{xy}}{\partial x} \\ + \frac{\partial R_{yy}}{\partial y} + \frac{\tau_y}{\rho} - \frac{\partial}{\partial x} (dT_{xy}) - \frac{\partial}{\partial y} (dT_{yy}) + \psi_y = 0 \end{aligned} \quad (1c)$$

Here, η is the surface elevation, (P, Q) is the depth-integrated velocity (the flux) in Cartesian coordinate system (x, y) , t is the time, $d = h + \eta$ is the total water depth and h is the still water depth.

The terms R_{xx} , R_{xy} and R_{yy} are additional convective momentum terms due to the inclusion of wave breaking and they are defined by

$$\begin{aligned} (R_{xx}, R_{xy}, R_{yy}) = \frac{\delta}{1 - \delta/d} \left(\left(c_x - \frac{P}{d} \right)^2, \left(c_x - \frac{P}{d} \right) \right. \\ \left. \times \left(c_y - \frac{Q}{d} \right), \left(c_y - \frac{Q}{d} \right)^2 \right) \end{aligned} \quad (2)$$

Here, $\delta = \delta(x, y, t)$ is the thickness of the surface roller and $c = (c_x, c_y)$ is the roller celerity. The determination of the roller thickness and the roller celerity is

described in Section 2.2. The bottom shear stress is modelled using

$$(\tau_x, \tau_y) = \frac{1}{2} f_m \frac{\sqrt{P^2 + Q^2}}{d^2} (P, Q) \quad (3)$$

where f_m is the friction factor. The turbulent mixing processes are modelled by means of an eddy viscosity formulation

$$\begin{aligned} T_{xx} &= 2v \frac{\partial}{\partial x} \left(\frac{P}{d} \right), \\ T_{xy} &= T_{yx} = v \left(\frac{\partial}{\partial y} \left(\frac{P}{d} \right) + \frac{\partial}{\partial x} \left(\frac{Q}{d} \right) \right), \\ T_{yy} &= 2v \frac{\partial}{\partial y} \left(\frac{Q}{d} \right) \end{aligned} \quad (4)$$

where v is the eddy viscosity. The eddy viscosity is estimated using the Smagorinsky formulation

$$v = l^2 s \left[\left(\frac{\partial U}{\partial x} \right)^2 + 2 \left(\frac{\partial U}{\partial y} + \frac{\partial V}{\partial x} \right)^2 + \left(\frac{\partial V}{\partial y} \right)^2 \right]^{1/2} \quad (5)$$

Here, s is the Smagorinsky coefficient, l is a characteristic length and U and V are components of the time-averaged wave-induced current field. The time-averaged velocity field is calculated using a second-order Butterworth low-pass filter. This is an efficient recursive filter that requires only values of the fluxes at the two previous time steps to be retained in memory. The use of a moving average filter for this purpose is not an attractive alternative as this would require a much larger buffer.

The terms ψ_x and ψ_y are dispersive Boussinesq-type terms. In the formulation by Madsen and Sørensen (1992), the dispersive terms include third-order derivatives of the surface elevation. The presence of higher-order spatial derivatives is one of the main problems when solving the Boussinesq equations using the finite element method. Therefore, the Boussinesq equations are rewritten in a lower-order form

by introducing a new auxiliary variable, w , and an auxiliary algebraic equation. Following the derivation by Madsen and Sørensen (1992), the starting point is the classical Boussinesq equations by Peregrine (1967). Using the mild-slope assumption, the dispersive terms can be written

$$\begin{aligned} \psi_x = & -\frac{1}{3}h^2 \left(\frac{\partial^3 P}{\partial x^2 \partial t} + \frac{\partial^3 Q}{\partial x \partial y \partial t} \right) \\ & - h \frac{\partial h}{\partial x} \left(\frac{1}{3} \frac{\partial^2 P}{\partial x \partial t} + \frac{1}{6} \frac{\partial^2 Q}{\partial y \partial t} \right) - h \frac{\partial h}{\partial y} \left(\frac{1}{6} \frac{\partial^2 Q}{\partial x \partial t} \right) \end{aligned} \quad (6a)$$

$$\begin{aligned} \psi_y = & -\frac{1}{3}h^2 \left(\frac{\partial^3 P}{\partial x \partial y \partial t} + \frac{\partial^3 Q}{\partial y^2 \partial t} \right) - h \frac{\partial h}{\partial x} \left(\frac{1}{6} \frac{\partial^2 P}{\partial y \partial t} \right) \\ & - h \frac{\partial h}{\partial y} \left(\frac{1}{6} \frac{\partial^2 P}{\partial x \partial t} + \frac{1}{3} \frac{\partial^2 Q}{\partial y \partial t} \right) \end{aligned} \quad (6b)$$

These terms can be modified using the linear long wave approximations

$$\frac{\partial P}{\partial t} + gh \frac{\partial \eta}{\partial x} \approx 0 \quad (7a)$$

$$\frac{\partial Q}{\partial t} + gh \frac{\partial \eta}{\partial y} \approx 0 \quad (7b)$$

By spatial differentiation and combination of these equations, we arrive at

$$\begin{aligned} \frac{\partial^3 P}{\partial x^2 \partial t} + \frac{\partial^3 Q}{\partial x \partial y \partial t} + \frac{\partial}{\partial x} \left(\frac{\partial}{\partial x} \left(gh \frac{\partial \eta}{\partial x} \right) \right) \\ + \frac{\partial}{\partial y} \left(gh \frac{\partial \eta}{\partial y} \right) \approx 0 \end{aligned} \quad (8a)$$

$$\begin{aligned} \frac{\partial^3 P}{\partial x \partial y \partial t} + \frac{\partial^3 Q}{\partial y^2 \partial t} + \frac{\partial}{\partial y} \left(\frac{\partial}{\partial x} \left(gh \frac{\partial \eta}{\partial x} \right) \right) \\ + \frac{\partial}{\partial y} \left(gh \frac{\partial \eta}{\partial y} \right) \approx 0 \end{aligned} \quad (8b)$$

The next step is to introduce a new auxiliary variable, w , defined by

$$w = \frac{\partial}{\partial x} \left(h \frac{\partial \eta}{\partial x} \right) + \frac{\partial}{\partial y} \left(h \frac{\partial \eta}{\partial y} \right) \quad (9)$$

Multiplying Eq. (8a) and Eq. (8b) with $-Bh^2$ and adding these to Eq. (6a) and Eq. (6b), respectively, finally yields the new Boussinesq equations. The dispersive terms become

$$\begin{aligned} \psi_x = & -\left(B + \frac{1}{3}\right)h^2 \left(\frac{\partial^3 P}{\partial x^2 \partial t} + \frac{\partial^3 Q}{\partial x \partial y \partial t} \right) \\ & - \frac{1}{6}h \frac{\partial h}{\partial x} \left(2 \frac{\partial^2 P}{\partial x \partial t} + \frac{\partial^2 Q}{\partial y \partial t} \right) \\ & - \frac{1}{6}h \frac{\partial h}{\partial y} \frac{\partial^2 Q}{\partial x \partial t} - Bgh^2 \frac{\partial w}{\partial x} \end{aligned} \quad (10a)$$

$$\begin{aligned} \psi_y = & -\left(B + \frac{1}{3}\right)h^2 \left(\frac{\partial^3 P}{\partial x \partial y \partial t} + \frac{\partial^3 Q}{\partial y^2 \partial t} \right) \\ & - \frac{1}{6}h \frac{\partial h}{\partial x} \frac{\partial^2 P}{\partial y \partial t} - \frac{1}{6}h \frac{\partial h}{\partial y} \left(\frac{\partial^2 P}{\partial x \partial t} + 2 \frac{\partial^2 Q}{\partial y \partial t} \right) \\ & - Bgh^2 \frac{\partial w}{\partial y} \end{aligned} \quad (10b)$$

This matches a mild-slope version of the equations derived in Section 2.1 of Schäffer and Madsen (1995) with their $B_2 = 0$. The free parameter B can be chosen as to optimize the dispersion characteristics. In the present work, $B = 1/15$ is applied.

2.2. Wave breaking

In the work by Schäffer et al. (1993), Madsen et al. (1997a,b) and Sørensen et al. (1998), the determination of the thickness of the surface roller relies on a heuristic, geometrical approach. The toe of the roller is defined as the location, where the local slope of the surface elevation is equal to a critical value, $\tan\phi$. Due to the transition from initial breaking to a bore-like stage in the inner surf zone, the critical angle, ϕ , is assumed to decrease from an initial breaking angle, ϕ_B , to a terminal breaking angle, ϕ_0 . Hence, breaking is initiated when the local slope exceeds $\tan\phi_B$, and breaking ceases when the maximum of the slope becomes less than $\tan\phi$. The value of the critical angle depends on the

age of the roller. The time variation of the critical breaking angle is modelled with an exponential decay

$$\tan\phi(t) = \tan\phi_0 + (\tan\phi_B - \tan\phi_0)\exp\left[-\ln 2 \frac{t - t_B}{t_{1/2}}\right] \quad (11)$$

where t_B is the time of incipient breaking and $t_{1/2}$ defines the time scale for the development of the roller. $t_{1/2}$ is determined as a fraction of a characteristic wave period, T . In one horizontal dimension, the roller thickness is determined as the water above the tangent of the slope, $\tan\phi$, starting at the roller toe point and pointing in the direction opposite to the direction of wave propagation. This thickness is multiplied by a factor, f_δ , prior to the inclusion in the governing equations. Hence, for waves propagating in the positive x direction, the roller thickness is given by

$$\delta = f_\delta(\eta - (\eta_r + (x_r - x)\tan\phi)) \quad (12)$$

where η_r is the surface elevation at the roller toe and x_r is the coordinate at the roller toe. In two horizontal dimensions, the toe of the roller becomes a curve instead of a point and the tangent becomes a tangential surface separating the roller from the rest of the flow.

While this geometrical approach is relatively simple when described in a continuous system, it becomes quite complicated in a discrete formulation in two horizontal dimensions. A much more simple technique can be obtained essentially by transforming the method to the time domain, where the original method was primarily operating in space. Assuming that the waves are of locally constant form (regular, progressive wave field), the following expression for the time derivative of the roller thickness can be obtained

$$\frac{\partial\delta}{\partial t} = f_\delta\left(\frac{\partial\eta}{\partial t} - c\tan\phi\right) \quad \text{and} \quad \delta \geq 0 \quad (13)$$

This formulation is suitable for one as well as two horizontal dimensions. Now, the initiation and cessa-

tion of wave breaking is determined based on threshold values for the time derivative of the surface elevation. A wave starts to break when the time derivative of the surface elevation exceeds $(\partial\eta/\partial t)_B = c\tan\phi_B$, and breaking will cease when it becomes less than $(\partial\eta/\partial t)_0 = c\tan\phi_0$. Obviously, breaking waves never obey the constant-form assumption exactly. However, since the starting point was no more than a simple, heuristic approach, there is no reason to believe that the new method is less appropriate than the original one. As demonstrated in Section 4.2, the two methods provide almost identical results. The formulation in Eq. (13) has the additional merit that it can be used with space marching techniques for wave evolution equations (see Bredmose et al., 2003).

As shown by Madsen et al. (1997a), the roller celerity can be determined interactively from the instantaneous wave field. However, this procedure may cause stability problems especially in two horizontal dimensions. Therefore, we have used the following approximation of the roller celerity

$$(c_x, c_y) = (c\cos\theta, c\sin\theta) \quad c = f_v\sqrt{gh} \\ \tan\theta = \frac{\partial\eta/\partial y}{\partial\eta/\partial x} \quad (14)$$

Using $f_v = 1.0$, we obtain the celerity determined by linear shallow water theory. This is often a rather good approximation just outside the surf zone, while $f_v = 1.3$ is more appropriate inside the surf zone (see the discussion in Madsen et al., 1997a). The transition from $f_v = 1.0$ to $f_v = 1.3$ is modelled with an exponential time variation. The time constant applied is the same as the one used for the time variation of the breaking angle.

In Madsen et al. (1997a), the default parameter set $(\phi_B, \phi_0, t_{1/2}, f_\delta) = (20^\circ, 10^\circ, T/5, 1.5)$ was suggested, and the parameter set was shown to give good results for both spilling and plunging breakers. This set of parameters has also been used in the present work. Kennedy et al. (2000) and Chen et al. (2000) also used a breaking criterion based on threshold values for the time derivatives of the surface elevation. They solved the equations by Wei et al. (1995) and used $(\partial\eta/\partial t)_B = 0.65\sqrt{gh}$ and $(\partial\eta/\partial t)_0 = 0.15\sqrt{gh}$. If the

roller celerity is estimated by Eq. (14) with $f_v = 1.0$ and 1.3, respectively, at the initiation and cessation of breaking, this corresponds to using $\phi_B = 33^\circ$ and $\phi_0 = 6.6^\circ$. The difference in the choice of values for ϕ_B and ϕ_0 is mainly due to the different linear and non-linear properties of the Boussinesq-type equations applied. The enhanced Boussinesq equations used in the present work underestimate the non-linear shoaling and wave height in the vicinity of the break point, while the use of the equation by Wei et al. can result in an overprediction of the non-linear shoaling.

2.3. Moving shoreline

The moving shoreline is modelled using the approach presented by Tao (1983) and Madsen et al. (1997a). Here, the solid beach is replaced by a permeable beach characterised by an extremely small porosity. The following vertical variation of the porosity is assumed

$$\gamma(z) = \begin{cases} 1 & Z_L \leq z \\ \varepsilon + (1 - \varepsilon)e^{\beta(z-Z_L)/(Z_L-Z_B)} & Z_B \leq z \leq Z_L \end{cases} \quad (15)$$

where ε is the minimum value of the porosity, β is a constant shape factor defining the exponential transition between the two regimes, z is the vertical coordinate, Z_L defines the physical seabed and Z_B defines the lower limit of the porous region. The porosity is introduced in the equations by replacing the total water depth in the momentum equations by the effective total water depth obtained by vertical integration of $\gamma(z)$ from Z_B to the free surface and by multiplying the time derivative of the surface elevation in Eq. (1a) by a representative porosity $\alpha = \gamma(\eta)$. The parameters used in the following are $\varepsilon = 0.005$ and $\beta = 100$. Inside the permeable beach ($h < 0$), the Boussinesq terms are switched off.

3. Numerical methods

3.1. Space discretisation

For the spatial discretisation, the standard Galerkin finite element method is applied. A description

of the basic theory of the Galerkin approach may be found, for example, in Zienkiewicz and Taylor (1989). The spatial domain Ω with boundary Γ is discretised by subdivision of the continuum into non-overlapping elements and defining a number of discrete nodes for each element. The finite element approximations of the dependent variables are

$$\begin{aligned} P(x, y) &\approx \sum_{i=1}^{N_1} p_i \phi_i(x, y) & Q(x, y) &\approx \sum_{i=1}^{N_1} q_i \phi_i(x, y) \\ \eta(x, y) &\approx \sum_{i=1}^{N_2} \eta_i \psi_i(x, y) & w(x, y) &\approx \sum_{i=1}^{N_2} w_i \psi_i(x, y) \end{aligned} \quad (16)$$

where p_i , q_i , η_i and w_i are the values of the dependent variables at the nodal points, ϕ_i and ψ_i are the standard basis functions and N_1 and N_2 are the total number of unknowns. The standard basis functions are locally defined polynomials. Finite element solutions of the Boussinesq equations in primitive form can exhibit severe spurious modes, especially when equal-order basis functions are applied for the velocities and the surface elevation. To get stable and oscillation free solutions, mixed interpolation is used in the present work. Both triangular elements (quadratic fluxes and linear surface elevation and auxiliary variable) and quadrilateral elements (biquadratic fluxes and bilinear surface elevation and auxiliary variable) are applied in the present work. The use of either triangular or quadrilateral elements or a combination of these increases the possibility to generate the optimal mesh for an actual case.

The governing equations are recasted into a weak form by multiplying Eqs. (1b) and (1c) with the weighting functions, ϕ_i , and Eqs. (1a) and (9) with the weighting functions, ψ_i , and integrating over the domain, Ω . Applying the divergence theorem, the equations can be written in a form which only requires the interpolation functions to be continuous. The integration by parts introduces integrals on the boundary, Γ . Introducing the finite element approximation for the dependent variables, the following system of differential/alge-

braic equations (DAEs) for the nodal unknowns is obtained

$$\begin{bmatrix} M_1 + B_1 & B_2 \\ B_3 & M_1 + B_4 \\ & & M_2 \end{bmatrix} \begin{pmatrix} \dot{p} \\ \dot{q} \\ \dot{\eta} \end{pmatrix} = \begin{pmatrix} g_1 \\ g_2 \\ g_3 \end{pmatrix} \quad (17a)$$

where

$$\begin{pmatrix} g_1 \\ g_2 \\ g_3 \end{pmatrix} = \begin{pmatrix} f_p \\ f_q \\ f_\eta \end{pmatrix} - \begin{bmatrix} N(p, q, h) & G_x \\ & N(p, q, h) & G_y \\ C_x & & C_y \end{bmatrix} \times \begin{pmatrix} p \\ q \\ \eta \end{pmatrix} - \begin{bmatrix} A_x \\ A_y \end{bmatrix} (w)$$

and

$$M_2 w = g_4 \quad (17b)$$

where

$$g_4 = f_w - Ds$$

Here (p, q, η) and $(\dot{p}, \dot{q}, \dot{\eta})$ are global vectors containing the nodal values and their time derivatives, respectively. w is a global vector containing the nodal values of the previous defined continuous variable, w (Eq. (9)). A description of the matrices and vectors in Eqs. (17a)–(17b) is presented in Appendix A. Global mass conservation is retained in the discrete finite element system when natural boundary conditions are enforced.

3.2. Time integration

The integration in time is performed using a three-step explicit Taylor–Galerkin method. Details of the method are given in Kashiwama et al. (1995). To

obtain the auxiliary variable and the derivatives with respect to time of the fluxes and surface elevation, three sets of linear equations have to be solved.

$$\begin{bmatrix} M_1 + B_1 & B_2 \\ B_3 & M_1 + B_4 \end{bmatrix} \begin{pmatrix} \dot{p} \\ \dot{q} \end{pmatrix} = \begin{pmatrix} g_1 \\ g_2 \end{pmatrix} \quad (18a)$$

$$M_2 \dot{\eta} = g_3 \quad (18b)$$

$$M_2 \dot{w} = g_4 \quad (18c)$$

For small problems, these systems can be solved using Gaussian elimination with sparse technique. However, for large systems, more cost-efficient methods must be applied such as a Krylov subspace iterative method (e.g., GMRES) combined with an efficient preconditioner (e.g., an incomplete LU factorisation). Both methods have been implemented in the present work. To further reduce the computational costs for large problems, the system of linear equations Eq. (18a) is solved using iteration

$$[M_1 + B_1] \dot{p}^{k+1} = g_1 - B_2 \dot{q}^k \quad (19a)$$

$$k = 1, 2, \dots$$

$$[M_1 + B_4] \dot{q}^{k+1} = g_2 - B_3 \dot{p}^{k+1} \quad (19b)$$

Only a few iterations are needed to obtain convergence. In the present work, the systems of linear equations Eqs. (18b)–(18c) and (19a)–(19b) are solved using GMRES with incomplete LU factorisation as preconditioner.

3.3. Boundary conditions

Three types of boundaries can be specified: A closed boundary (a fully reflecting wall), an open flux boundary and a fully absorbing boundary. At a flux boundary, we have

$$p_n = p n_x + q n_y = p_n^*$$

and

$$\frac{\partial \eta}{\partial n} = \frac{\partial \eta}{\partial x} n_x + \frac{\partial \eta}{\partial y} n_y = \left(\frac{\partial \eta}{\partial n} \right)^* \quad (20)$$

where p_n^* and $(\partial \eta / \partial n)^*$ are known values from the incident wave condition at the open boundary and

$n=(n_x, n_y)$ is the unit outward normal vector. For waves of constant form on horizontal bottom, p_n^* and $(\partial\eta/\partial n)^*$ can be expressed in terms of the surface elevation, the wave frequency and the wave number. Hence, by using Fourier series decomposition technique, p_n^* and $(\partial\eta/\partial n)^*$ can be determined for any linear irregular surface elevation variation. A closed boundary is the special case, where

$$p^* = 0 \text{ and } \left(\frac{\partial\eta}{\partial n}\right)^* = 0 \quad (21)$$

At both a closed boundary and an open flux boundary, the boundary conditions are implemented by solving the tangential momentum equation together with the equation $p_n = p^*$ following the approach by Engelman et al. (1982). Note that for the tangential momentum equations

$$t_x f_p + t_y f_q \equiv 0 \quad (22)$$

Hence, the boundary integrals cancel out exactly. At a closed boundary, the boundary integral, f_η and f_w , are identical to zero, while these two integrals must be calculated at an open boundary. A fully absorbing

boundary is simulated using the sponge-layer approach. In the sponge layers, an explicit damping of both the surface elevation and the fluxes is performed after each time step. The damping coefficients are close to unit along the front of the sponge layer and are increasing smoothly towards the boundary.

4. Numerical experiments

In order to verify the accuracy of the numerical approach and to validate the model, the model is applied to four test cases.

4.1. Non-linear refraction–diffraction of regular waves over a semicircular shoal

The first test case is the non-linear refraction–diffraction of regular waves over a semicircular shoal. The problem was studied experimentally by Whalin (1971). For a presentation of numerical results, see, e.g., Madsen and Sørensen (1992) and the references herein. Whalin performed a series of experiments with different wave conditions. Here, we concentrate on the case with a wave period of 2 s and a wave amplitude

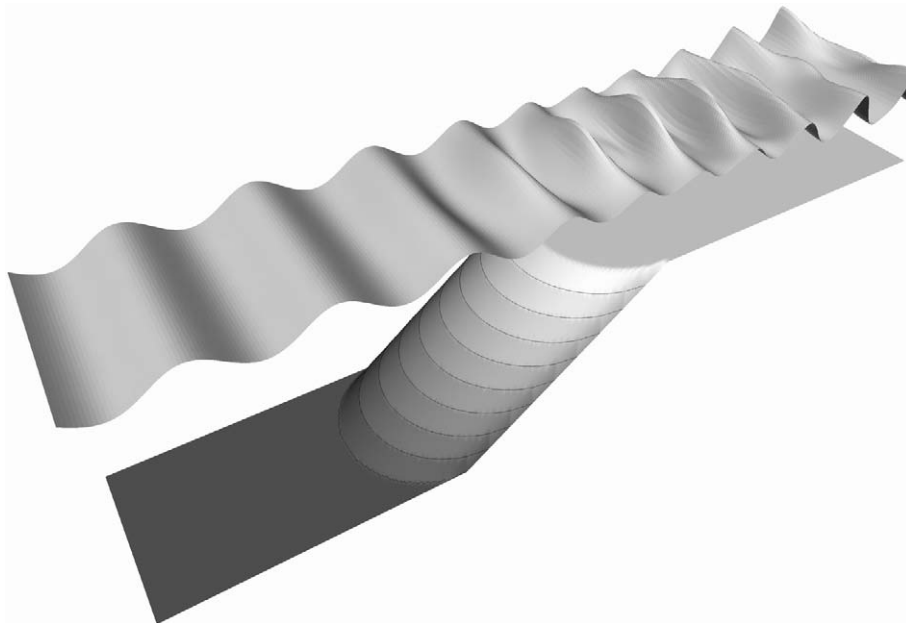


Fig. 1. Instantaneous surface elevation calculated using the new FEM model shown over the bathymetry.

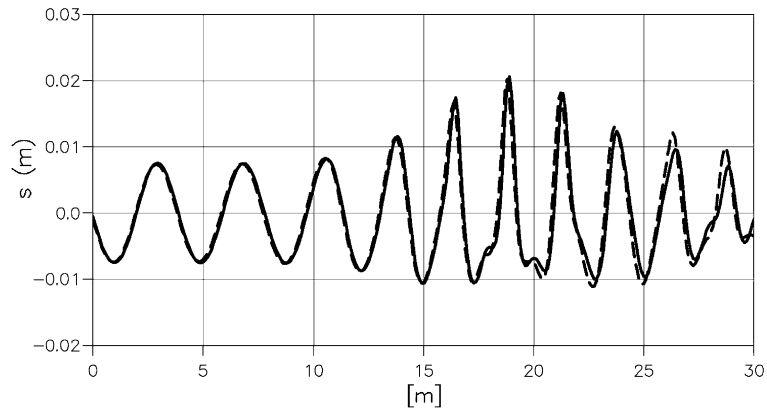


Fig. 2. Surface elevation along the centreline ($T=2$ s and $H=0.015$ m). (—) New model (FEM); (- - -) existing model (FDM).

of 0.0075 m. The model area covers 6.096×36.576 m with a depth variation given by

$$h(x,y) = \begin{cases} 0.4572 & 0 \leq x \leq 10.67 - G \\ 0.4572 + \frac{1}{25}(10.67 - G - x) & 10.67 - G \leq x \leq 18.29 - G \\ 0.1524 & 18.29 - G \leq x \leq 36.576 \end{cases}$$

where

$$G(y) = [y(6.096 - y)]^{1/2} \quad 0 \leq y \leq 6.096$$

The results using the new model are compared to both experimental data and to the results obtained using an existing Boussinesq model based on the FDM. A detailed description of the latter can be found in Madsen et al. (1991) and Madsen and Sørensen (1992). Note that both the new and the existing model are based on the enhanced Boussinesq equations with Padé [2,2] dispersion.

For the new model, quadrilateral elements with an edge length of 0.1016 m are used, resulting in 21 600 elements. The number of nodes is 22 021 and 87 241, respectively, for the linear and quadratic interpolation. For the existing model, a grid spacing of 0.1016 m is used resulting in 21 600 discrete unknowns for the surface elevation. A time step of 0.02 and 0.01 s is applied for the new and the existing model, respectively. The small time step is needed for the existing model to get a stable solution due to the treatment of the Boussinesq terms. For the existing model, a time step of 0.02 s is applied while for the new model a time step of 0.01 s must be applied due to the

biquadratic interpolation of the fluxes. The outgoing waves at the downstream boundary are absorbed using a 6-m-wide sponge layer.

The incoming waves are linear, but after the focusing on the shoal, higher harmonics become significant due to non-linear effects. The focusing of the waves can be seen in Fig. 1 showing an instantaneous surface elevation field calculated using the new FEM model. Fig. 2 shows the surface elevation along the centreline. The energy transfer to higher harmonics is illustrated in Fig. 3. Based on a Fourier analysis of the time series of surface elevation at each grid point along the centreline, the spatial evolution of the first, second and third harmonics from the numerical simulations is compared with the experimental data.

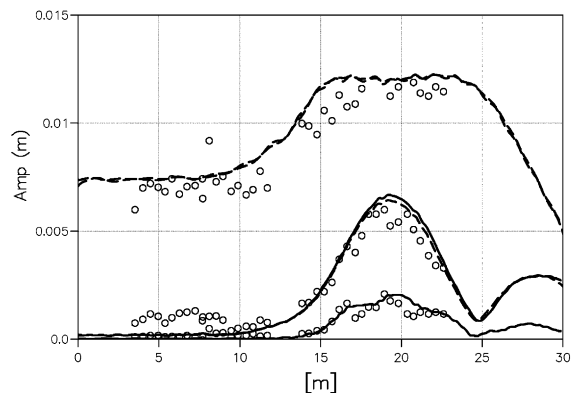


Fig. 3. Wave amplitude for the first, second and third harmonic along the centreline ($T=2$ s and $H=0.015$ m). (—) New model (FEM); (- - -) existing model (FDM); (o) experimental data by Whalin (1971).

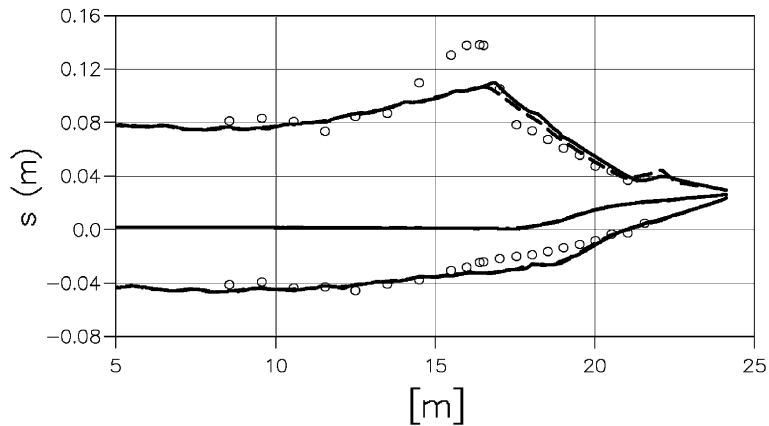


Fig. 4. Spatial variation of wave crest elevation, wave trough elevation and mean water level for regular waves breaking on a gently sloping beach. (—) Old breaking procedure; (- - -) new breaking procedure (o); experimental data by Ting and Kirby (1994).

The results from the two numerical models are almost identical and the agreement with the measurements is quite good.

4.2. Shoaling and breaking of regular waves on a gently sloping beach

The two different procedures for determination of the roller thickness (see Section 2.2) are compared for the shoaling and breaking of regular waves on a gently sloping beach. Ting and Kirby (1994) presented measurements for spilling breakers on a plane sloping beach with a slope of 1/35 starting at a depth

of 0.40 m. As input, they generated regular waves with a period of 2.0 s and a wave height of 0.121 m. This test case is a one-dimensional flow problem. Hence, a one-element wide channel is used in the simulation. Quadrilateral elements with an edge length of 0.02 m are used. For comparison a one-dimensional version of the finite element model using the old procedure for determination of the roller thickness is also applied. In both cases, the time step is 0.005 s.

The cross-shore variation of the wave crest elevation, wave trough elevation and mean water level are shown in Fig. 4 and the cross-shore variation of the

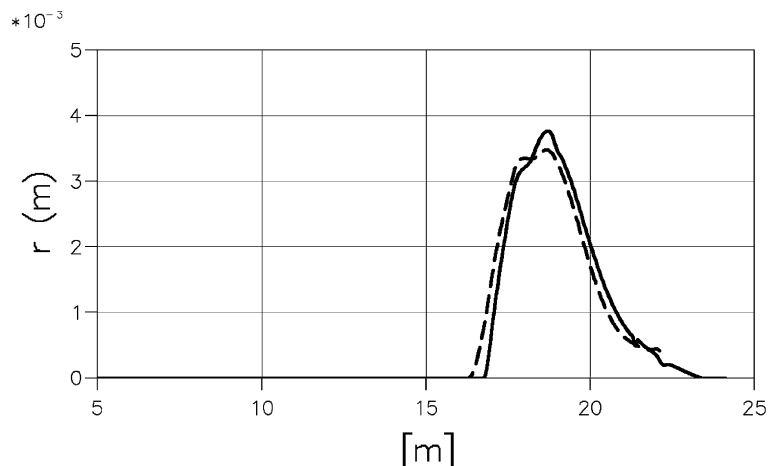


Fig. 5. Spatial variation of mean roller thickness. (—) Old breaking procedure; (- - -) new breaking procedure.

mean roller thickness is shown in Fig. 5. It can be seen that the new and the old procedures for calculation of the roller thickness give almost identical results. The pronounced shoaling just up to the break point is significantly underestimated. The reason for this discrepancy is that the enhanced Boussinesq equations underestimate the transfer of energy to the superharmonics.

4.3. Shoaling and breaking of irregular waves on a gently sloping beach

The simulation of shoaling, breaking and runup of irregular waves are verified by comparing with the experimental results reported by Cox et al. (1991). The physical flume consists of a 10-m horizontal section with a water depth of 0.47 m and a 12-m section with a constant 1/20 impermeable slope. An incident wave spectrum of Pierson–Moskowitz type

with a peak period of 1.0 s and a significant wave height of 6.45 cm is considered.

The mesh consists of quadrilateral elements. The mesh is one element wide, and along the flume, it is adapted to the wavelength. The element size in the cross-shore direction is chosen, so that a wave with a characteristic wave period of 1 s is resolved with 40 elements per wavelength. The maximum edge length is 0.0375 m and the minimum edge length is set to 0.01 m. The edge length in the longshore direction is 0.0375 m. The time step is 0.04 s.

The incoming waves are specified using an internal boundary at a water depth of 0.25 m. The measured surface elevation at this depth is analysed by a Fourier analysis, the low frequency motion ($f < 0.1$ Hz) is removed and the remaining signal is converted into a flux condition. At the offshore boundary, a 1-m-wide sponge layer is placed to absorb the outgoing waves.

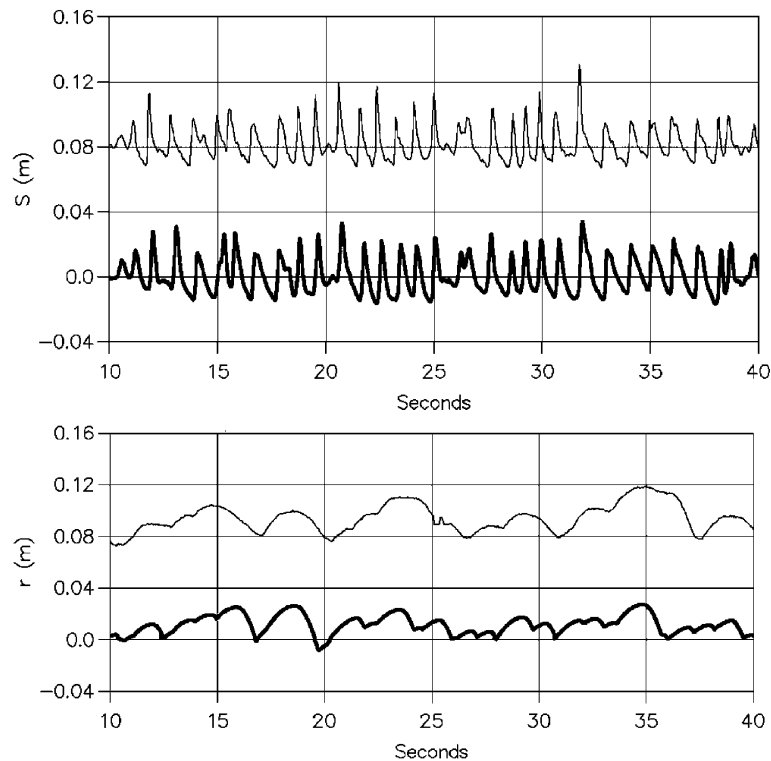


Fig. 6. Time series of surface elevation (S) and swash oscillation (r , vertical displacement). (—) Present model; (—) experimental data by Cox et al. (1991), shifted relative to the computed results by 0.08 m.

Fig. 6 shows a comparison between the FEM results and the measurements. The top panel shows the surface elevation at a still water depth of 5 cm (wave gauge 11), which is well inside the breaking zone. The bottom panel shows the motion of the shoreline converted into vertical displacement. The agreement is seen to be quite good. The shoreline motion is dominated by low frequency oscillations, which is to be expected because the wave breaking for this case is dominated by spilling breakers. The resemblance between measurements and model results is similar to what was previously reported using a finite difference model, see Madsen et al. (1997b).

4.4. Rip channel

Laboratory experiments for a case with waves propagation on a plane beach with a rip channel have been reported by Hamm (1992a,b). The wave basin is 30×30 m and the bathymetry is a plane sloping

beach of 1:30 with a rip channel excavated along the centreline. The depth variation is given by

$$h(x,y) = \begin{cases} 0.5 & x \leq 7 \\ -0.1 + \frac{25-x}{30} \left[1 + 3 \exp\left(-\frac{25-x}{30}\right) \cos^{10}\left(\frac{\pi(15-y)}{30}\right) \right] & 7 < x < 25 \\ -0.1 + \frac{25-x}{30} & x \leq 25 \end{cases}$$

Hamm considered a number of different incident wave conditions. Here, the case with unidirectional, regular, incident waves with a period of 1.25 s and a wave height of 0.07 m is considered.

Only half of the physical wave tank is covered in the computations, and reflective boundary conditions are applied at the line of symmetry. The mesh is generated using a triangular mesh generator based on constrained Delaunay triangulation. The first step in the mesh generation is to generate a basic mesh based on the nodes specifying the boundary of the computational domain. The next step is to refine the mesh by imposing constraints on minimum angle and maximum triangle area. A depth-adaptive mesh can be

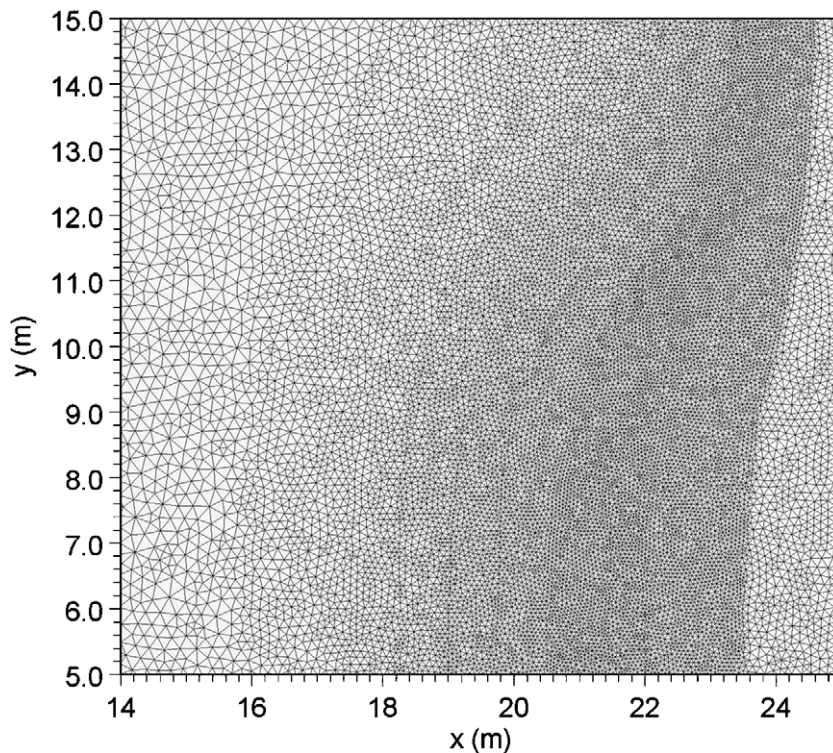


Fig. 7. Close up of the mesh.

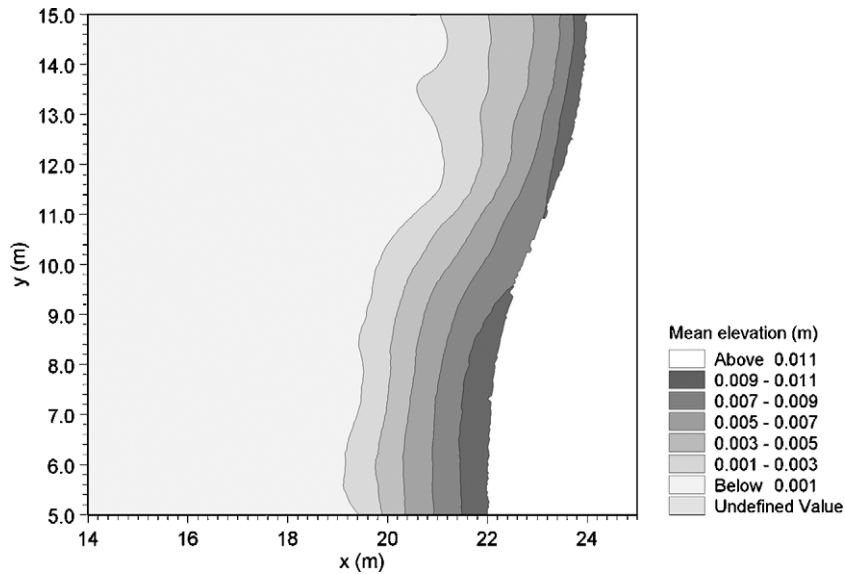


Fig. 8. Contour plot of the mean surface elevation.

constructed by making the constraint on maximum area depend on the local water depth. A depth-adaptive unstructured mesh is used with 62 635 triangular elements (125 852 nodes for the velocity and 31 609 nodes for the surface elevation). At the off-

shore boundary, the element size is approximately 0.02 m^2 while the element size near the shoreline is around 0.00125 m^2 . Inside the permeable beach, the element size is 0.02 m^2 . The minimum angle is 26° . A close up of the mesh is shown in Fig. 7. The time step

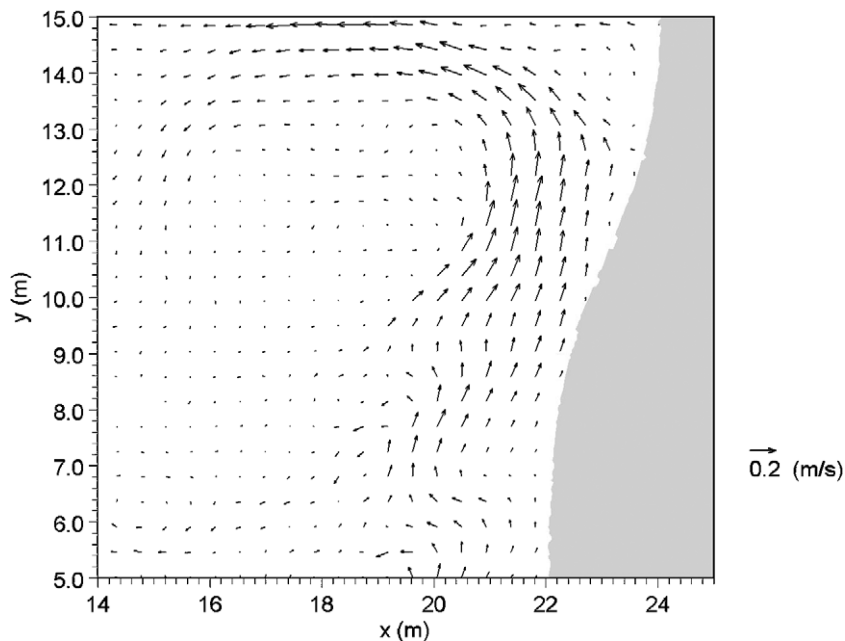


Fig. 9. Vector plot of the time-averaged velocity field.

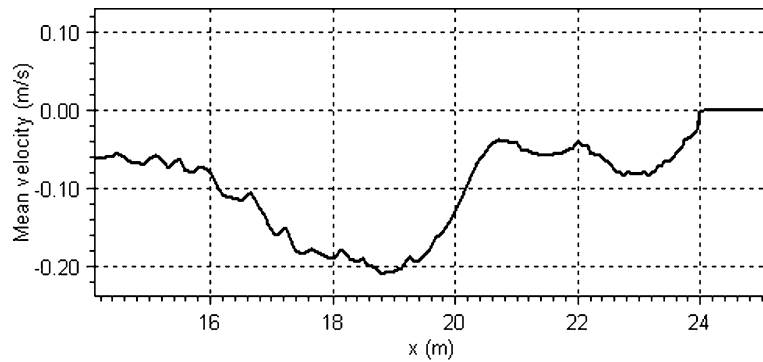


Fig. 10. Rip current along the centreline.

is 0.015 s and the simulation period is 450 s corresponding to 360 wave periods. Note that if a Cartesian mesh is used with an element size of 0.00125 m^2 , then 360 000 elements are needed. Hence, the number of elements is reduced with a factor 6 for this case using an unstructured depth-adaptive mesh instead of a Cartesian mesh. A constant friction factor of $f_w = 0.03$ is used in the bed friction term and a Smagorinsky coefficient of $s = 0.1$ is used.

Due to the difference in the wave set-up along the rip channel, and at the plane beach away from the rip channel, there is an alongshore gradient in the mean water surface elevation. This gradient will force a current towards the centreline. The flow from both sides will join to form a rip current and two symmetrical circulation cells will be created. A steady-state current field will be reached when the forcing due to

the gradient in the mean surface elevation is balanced out by the bed friction.

In the numerical simulation, the steady-state wave-induced current field is reached after approximately 120 wave periods (150 s). A contour plot of the mean surface elevation is shown in Fig. 8 and a vector plot of the time-averaged velocity field is shown in Fig. 9. A subdomain is shown in order to focus on the circulation cell. The velocity is computed as the time-average of the depth-average velocity below the roller, u_0 . The velocity vectors are shown in a structured grid (with a resolution of 0.5 m). A pronounced rip current is seen along the centreline of the bathymetry, i.e., at the top of the figure. A formation of small eddies along the plane beach can also be identified. However, more detailed data are needed in order to show if similar eddies are actually present in

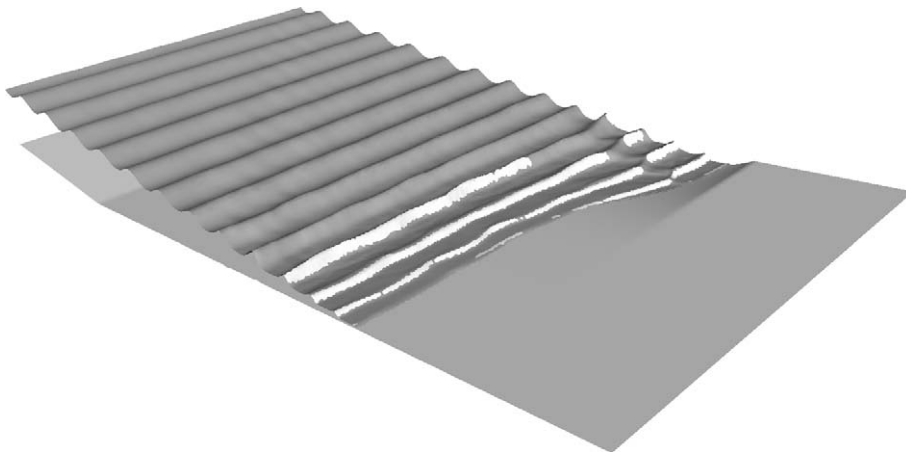


Fig. 11. Instantaneous surface elevation shown over the bathymetry.

the physical experiment. The cross-shore variation of the velocity along the centreline is shown in Fig. 10. The maximum velocity is 0.21 m/s, which corresponds well with the maximum measured value of 0.25 m/s.

A snapshot of the instantaneous surface elevation is shown in Fig. 11. It can be seen that the rip current significantly affects the wave motion. The large opposing rip current causes an increase in the wave height and a small local bend in the wave crest.

5. Conclusion

A numerical model for solving a set of extended time domain Boussinesq-type equations including the breaking zone and the swash zone has been presented. The model is based on the unstructured finite element technique. A new procedure for determination of the roller thickness has been devised. This provides a substantial simplification over the previously used procedure. The two procedures give almost the same results for spilling as well as plunging type of breaking.

The model has been applied to a number of test cases, and comparisons with an existing finite difference Boussinesq model and laboratory measurements show good agreement. The present work has shown the new model as an accurate tool for prediction of wave conditions in large coastal areas that include the surf zone.

The use of unstructured meshes offers the possibility of adapting the mesh resolution to the local physical scale. Compared to the use of structured meshes, the use of unstructured meshes may significantly reduce the number of nodes in the spatial discretisation, especially for the cases where the breaking and surf zone are included. The reduction which can be obtained will depend on the actual case and the optimization of the mesh. However, for large coastal areas where the breaking and surf zone are only a small part of the computational domain a reduction factor of 10–20 is realistic. Hence, the model has the potential to be a very cost-efficient tool. At this stage, however, the computational cost for a real-case study is still very large. The main computational task is to solve the linear system of equations at each time step. Therefore, the use of more

efficient solvers has to be investigated. Essential for application of the model for real-case studies is also further development of methods for generation of unstructured meshes.

Acknowledgements

This research was partly funded by The Danish Technical Research Council (STVF Grant No. 9801635) under the frame program Computational Hydrodynamics. Their financial support is greatly appreciated.

Appendix A

The matrices in Eqs. (17a) and (17b) are defined by:

The mass matrices

$$M_{1,ij} \equiv \int_{\Omega} \phi_i \phi_j d\Omega \quad i, j = 1, 2, \dots, N_1$$

$$M_{2,ij} \equiv \int_{\Omega} \psi_i \psi_j d\Omega \quad i, j = 1, 2, \dots, N_2$$

The advection matrix

$$N_{ij} \equiv \int_{\Omega} \left[\frac{p}{d} \frac{\partial \phi_j}{\partial x} + \frac{\partial}{\partial x} \left(\frac{p}{d} \right) \phi_j + \frac{q}{d} \frac{\partial \phi_j}{\partial y} + \frac{\partial}{\partial y} \left(\frac{q}{d} \right) \phi_j \right] \phi_i d\Omega \quad i, j = 1, 2, \dots, N_1$$

The elevation gradient matrices

$$G_{x,ij} \equiv \int_{\Omega} g d \frac{\partial \psi_j}{\partial x} \phi_i d\Omega$$

$$i = 1, 2, \dots, N_1, \quad j = 1, 2, \dots, N_2$$

$$G_{y,ij} \equiv \int_{\Omega} g d \frac{\partial \psi_j}{\partial y} \phi_i d\Omega$$

$$i = 1, 2, \dots, N_1, \quad j = 1, 2, \dots, N_2$$

The flux gradient matrices

$$C_{x,ij} \equiv - \int_{\Omega} \phi_j \frac{\partial \psi_i}{\partial x} d\Omega$$

$$i = 1, 2, \dots, N_2, \quad j = 1, 2, \dots, N_1$$

$$C_{y,ij} \equiv - \int_{\Omega} \phi_j \frac{\partial \psi_i}{\partial y} d\Omega$$

$$i = 1, 2, \dots, N_2, \quad j = 1, 2, \dots, N_1$$

The Boussinesq matrices

$$B_{1,ij} \equiv \int_{\Omega} \left(B + \frac{1}{3} \right) h^2 \frac{\partial \phi_j}{\partial x} \frac{\partial \phi_i}{\partial x} d\Omega + \int_{\Omega} \left(2B + \frac{1}{3} \right) h \frac{\partial h}{\partial x} \frac{\partial \phi_j}{\partial x} \phi_i d\Omega$$

$$i, j = 1, 2, \dots, N_1$$

$$B_{2,ij} \equiv \int_{\Omega} \left(B + \frac{1}{3} \right) h^2 \frac{\partial \phi_j}{\partial y} \frac{\partial \phi_i}{\partial x} d\Omega + \int_{\Omega} \left(\left(2B + \frac{1}{2} \right) h \frac{\partial h}{\partial x} \frac{\partial \phi_j}{\partial y} - \frac{1}{6} h \frac{\partial h}{\partial y} \frac{\partial \phi_j}{\partial x} \right) \phi_i d\Omega \quad i, j = 1, 2, \dots, N_1$$

$$B_{3,ij} \equiv \int_{\Omega} \left(B + \frac{1}{3} \right) h^2 \frac{\partial \phi_j}{\partial x} \frac{\partial \phi_i}{\partial y} d\Omega + \int_{\Omega} \left(-\frac{1}{6} h \frac{\partial h}{\partial x} \frac{\partial \phi_j}{\partial y} + \left(2B + \frac{1}{2} \right) \times h \frac{\partial h}{\partial y} \frac{\partial \phi_j}{\partial x} \right) \phi_i d\Omega \quad i, j = 1, 2, \dots, N_1$$

$$B_{4,ij} \equiv \int_{\Omega} \left(B + \frac{1}{3} \right) h^2 \frac{\partial \phi_j}{\partial y} \frac{\partial \phi_i}{\partial y} d\Omega + \int_{\Omega} \left(2B + \frac{1}{3} \right) h \frac{\partial h}{\partial y} \frac{\partial \phi_j}{\partial y} \phi_i d\Omega$$

$$i, j = 1, 2, \dots, N_1$$

$$A_{x,ij} \equiv \int_{\Omega} Bg\psi_j \left(h^2 \frac{\partial \phi_i}{\partial x} + 2h \frac{\partial h}{\partial x} \phi_i \right) d\Omega$$

$$i = 1, 2, \dots, N_1, \quad j = 1, 2, \dots, N_2$$

$$A_{y,ij} \equiv \int_{\Omega} Bg\psi_j \left(h^2 \frac{\partial \phi_i}{\partial y} + 2h \frac{\partial h}{\partial y} \phi_i \right) d\Omega$$

$$i = 1, 2, \dots, N_1, \quad j = 1, 2, \dots, N_2$$

$$D_{ij} \equiv \int_{\Omega} h \left(\frac{\partial \psi_j}{\partial x} \frac{\partial \psi_i}{\partial y} + \frac{\partial \psi_j}{\partial y} \frac{\partial \psi_i}{\partial x} \right) d\Omega$$

$$i, j = 1, 2, \dots, N_2$$

The vectors in Eqs. (17a) and (17b) contain the boundary integrals

$$f_p \equiv \int_{\Gamma} \left(B + \frac{1}{3} \right) h^2 \frac{\partial p}{\partial x} n_x \phi_i ds + \int_{\Gamma} \left(B + \frac{1}{3} \right) h^2 \frac{\partial q}{\partial y} n_x \phi_i ds + \int_{\Gamma} Bgh^2 w n_x \phi_i ds$$

$$f_q \equiv \int_{\Gamma} \left(B + \frac{1}{3} \right) h^2 \frac{\partial p}{\partial x} n_y \phi_i ds + \int_{\Gamma} \left(B + \frac{1}{3} \right) h^2 \frac{\partial q}{\partial y} n_y \phi_i ds + \int_{\Gamma} Bgh^2 w n_y \phi_i ds$$

$$f_{\eta} \equiv - \int_{\Gamma} (pn_x + qn_y) \phi_i ds$$

$$f_w \equiv \int_{\Gamma} h \left(\frac{\partial \eta}{\partial x} n_x + \frac{\partial \eta}{\partial y} n_y \right) \phi_i ds$$

where $n = (n_x, n_y)$ is the unit outward normal vector. For simplicity, the terms due to breaking, bottom

friction and turbulent mixing have been omitted. The domain integrals are calculated using isoparametric coordinate transformation and Gaussian quadrature.

References

- Antunes Do Carmo, J.S., Seabra-Santos, F.J., 1996. On breaking waves and wave-current interaction in shallow water: a 2DH finite element model. *Int. J. Numer. Methods Fluids* 22, 429–444.
- Beji, S., Nadaoka, K., 1996. A formal derivation and numerical modelling of the improved Boussinesq equations for varying depth. *Ocean Eng.* 23 (8), 691–704.
- Bredmose, H., Schäffer, H.A., Madsen, P.A., 2003. A roller breaking model for deterministic evolution equations, submitted for publication.
- Chen, Q., Kirby, J.T., Dalrymple, R.A., Kennedy, B.A., Chawla, A., 2000. Boussinesq modelling of wave transformation, breaking, and runup: II. 2D. *J. Waterw. Port Coast. Ocean Eng., ASCE* 126 (1), 57–62.
- Cox, D.T., Mase, H., Sakai, T., 1991. An experiment on the effect of fluid acceleration on seabed stability, Report No 91-Hy-01, Kyoto University, Japan.
- Engelman, M.S., Sani, J.L., Gresho, P.M., 1982. The implementation of normal and/or tangential boundary condition in finite element codes for incompressible fluid flows. *Int. J. Numer. Methods Fluids* 2, 225–238.
- Hamm, L., 1992a. Directional nearshore wave propagation over a rip channel: an experiment. *Proc. 23rd Int. Conf. Coastal Eng., ASCE, Venice, Italy*, 226–239.
- Hamm, L., 1992b. Random wave propagation in the nearshore zone: experiments in a directional wave basin, Internal Report, MAST-G6M, SOGREAH.
- Kashiyama, K., Ito, H., Behr, M., Tezduyar, T., 1995. Three-step explicit finite element computation of shallow water flows on a massively parallel computer. *Int. J. Numer. Methods Fluids* 21, 885–900.
- Kennedy, A.B., Chen, Q., Kirby, J.T., Dalrymple, R.A., 2000. Boussinesq modelling of wave transformation, breaking, and runup: I. 1D. *J. Waterw. Port Coast. Ocean Eng., ASCE* 126 (1), 39–47.
- Kirby, J.T., 1997. Nonlinear, dispersive long waves in water of variable depth. In: Hunt, J.N. (Ed.), *Gravity Waves in Water of Finite Depth. Advances in Fluid Mechanics*, vol. 10. Computational Mechanics Publications, Southampton, pp. 55–125.
- Kirby, J.T., 2003. Boussinesq models and applications to nearshore wave propagation, surf zone processes and wave-induced currents. In: Lakhan, C. (Ed.), *Advances in Coastal Engineering*. Elsevier, Amsterdam.
- Langtangen, H.P., Pedersen, G., 1998. Computational models for weakly dispersive non-linear water waves. *Comput. Methods Appl. Mech. Eng.* 160, 337–358.
- Li, Y.S., Zhan, J.M., 2001. Boussinesq-type model with boundary-fitted coordinate system. *J. Waterw. Port Coast. Ocean Eng., ASCE* 127, 152–160.
- Li, Y.S., Liu, S.-X., Lai, G.-Z., 1999. Numerical modeling of Boussinesq equations by finite element method. *Coast. Eng.* 37, 97–122.
- Li, Y.S., Liu, S.-X., Yu, Y.-X., Lai, G.-Z., 2000. Numerical modeling of multi-directional irregular waves through breakwaters. *Appl. Math. Model.* 24, 551–574.
- Löhner, R., Morgan, K., Zienkiewicz, O., 1984. The solution of non-linear hyperbolic equation systems by the finite element method. *Int. J. Numer. Methods Fluids* 4, 1043–1063.
- Madsen, P.A., Sørensen, O.R., 1992. A new form of the Boussinesq equations with improved linear dispersion characteristic: part II. A slowly-varying bathymetry. *Coast. Eng.* 18, 183–204.
- Madsen, P.A., Schäffer, H.A., 1999. A review of Boussinesq-type equations for surface gravity waves. In: Liu, P.L.-F. (Ed.), *Advances in Coastal and Ocean Engineering*, vol. 5. World Scientific Publ., pp. 1–95.
- Madsen, P.A., Murray, R., Sørensen, O.R., 1991. A new form of the Boussinesq equations with improved linear dispersion characteristics: part I. *Coast. Eng.* 15, 371–388.
- Madsen, P.A., Schäffer, H.A., Sørensen, O.R., 1997a. Surf zone dynamics simulated by a Boussinesq type model: part 1. Model description and cross-shore motion of regular waves. *Coast. Eng.* 32, 255–287.
- Madsen, P.A., Sørensen, O.R., Schäffer, H.A., 1997b. Surf zone dynamics simulated by a Boussinesq type model: part 2. Surf beat and swash oscillations for wave groups and irregular waves. *Coast. Eng.* 32 (4), 289–319.
- Nwogu, O., 1993. Alternative form of Boussinesq equations for nearshore wave propagation. *J. Waterw. Port Coast. Ocean Eng., ASCE* 119 (6), 618–638.
- Peraire, J., Zienkiewicz, O.R., Morgan, K., 1986. Shallow water problems: a general explicit formulation. *Int. J. Numer. Methods Eng.* 22, 547–574.
- Peregrine, D.H., 1967. Long waves on a beach. *J. Fluid Mech.* 27, 815–827.
- Schäffer, H.A., Madsen, P.A., 1995. Further enhancements of Boussinesq-type equations. *Coast. Eng.* 26, 1–14.
- Schäffer, H.A., Madsen, P.A., Deigaard, R., 1993. A Boussinesq model for waves breaking in shallow water. *Coast. Eng.* 20 (3/4), 185–202.
- Shi, F., Dalrymple, R.A., Kirby, J.T., Chen, Q., Kennedy, A., 2001. A fully nonlinear Boussinesq model in generalized curvilinear coordinates. *Coast. Eng.* 42, 337–358.
- Sørensen, O.R., Schäffer, H.A., Madsen, P.A., 1998. Surf zone dynamics simulated by a Boussinesq type model: Part III. Wave-induced horizontal nearshore circulations. *Coast. Eng.* 33, 155–176.
- Tao, J., 1983. Computation of wave run-up and wave breaking, Internal Report, Danish Hydraulic Institute, 40 pp.
- Ting, F.C.K., Kirby, J.T., 1994. Observation of undertow and turbulence in a laboratory surf zone. *Coast. Eng.* 24, 51–80.
- Whalin, R.W., 1971. The limit of applicability of linear wave refraction theory in convergence zone, Res. Rep. H-71-3, U.S. Army Corps of Engineers, Waterways Expt. Station, Vicksburg, MS.

- Walkley, M., Berzins, M., 1999. A finite element method for the one-dimensional extended Boussinesq equations. *Int. J. Numer. Methods Fluids* 29, 143–157.
- Walkley, M., Berzins, M., 2002. A finite element method for the two-dimensional extended Boussinesq equations. *Int. J. Numer. Methods Fluids* 39, 865–885.
- Wei, G., Kirby, J.T., Grilli, S.T., Subramanya, R., 1995. A fully nonlinear Boussinesq model for surface waves: I. Highly nonlinear unsteady waves. *J. Fluid Mech.* 294, 71–92.
- Zienkiewicz, O., Taylor, R., 1989. *The Finite Element Method*. McGraw-Hill, New York.